Direct Thrust Measurements of the HIPATIA System Thruster Unit

IEPC-2022-491

Presented at the 37th International Electric Propulsion Conference
Massachusetts Institute of Technology, Cambridge, MA, USA
June 19-23, 2022

Víctor Gómez[1], Mick Wijnen[2] and Jaume Navarro-Cavallé[3]
Universidad Carlos III de Madrid, Equipo de Propulsión Espacial y Plasmas, 28911 Leganés, Madrid, Spain

This work presents direct thrust measurements in a Helicon Plasma Thruster breadboard model, developed in the frame of the HIPATIA - H2020 Project. Thrust is measured for a wide range of mass flow rate, 12.5 to 40 sccm of Xenon, and radio-frequency power, 200-450 W. Besides, the thruster is powered by two different power electronics architectures presenting similar results for both of them. For the analyzed range, thrust scales up with power and mass flow rate, while the specific impulse drops with the increase of the mass flow rate. Thrust measurements spreads from 2.5 up to 6.5 mN, while the specific impulse is always lower than 400 s. This gain of thrust with power and mass flow rate do not impact on the thrust efficiency, instead, this remains almost constant and bounded between 1 and 2 %, meaning that related losses, i.e. ionization/excitation and plasma wall losses, increase as well with power and mass flow, almost at the same rate.

I. Introduction

The tremendous growth shown by the space market in the last decade has been accompanied and enabled partially by the development of the different subsystems that compose any spacecraft. Among them, the propulsion subsystem is essential for the success of most of the space missions. Within the family of electrical thrusters [8], gridded ion thrusters (GIT) and Hall thrusters (HT) have the hegemony in the realm of geostationary telecommunication satellites. These thrusters are of electrostatic nature, thus implying the unavoidable use of exposed electrodes to the plasma, shaped as grids, electron guns or neutralizers as well as anode surfaces, etc.; these elements have been reported [6, 1, 2] as the drivers for their shorten lifetime, although these already overpass several thousands of hours of firing [3]. The Electric Propulsion community has shown a drifting towards the development of electrodeless plasma thrusters in order to overcome the aforementioned lifetime limitation. We can find among them some potential candidates, the Electron Cyclotron Resonance (ECR) thruster [12] and the radiofrequency or Helicon plasma thrusters (HPT) [15, 20, 19]. The latest is a quite promising technology due to its additional presumable advantages over the already consolidated technologies: simplicity, propellant agnosticism, and ease of operation, i.e. the associated propellant management unit as well as the power processing unit are expected to be much simpler, and with less thruster elements to be controlled. Besides, some HPT prototypes have demonstrated a thruster unit efficiency overpassing the threshold of the 15 % [18].

The direct measurement of the thrust produced by these thrusters, which determines their thrust efficiency [15, 21], together with the analysis of plasma properties [7, 16, 17, 10], is key for the assessment of its maturity level and their potential to become a disruptive technology for in-space electric propulsion. In this work we will focus on the mapping of the thrust produced by an elegant breadboard model of a HPT unit when the operating parameters are modified.

[1]PhD candidate, Plasma and Space Propulsion Team
[2]PhD candidate
[3]Visiting Professor, corresponding author, janavarr@ing.uc3m.es.

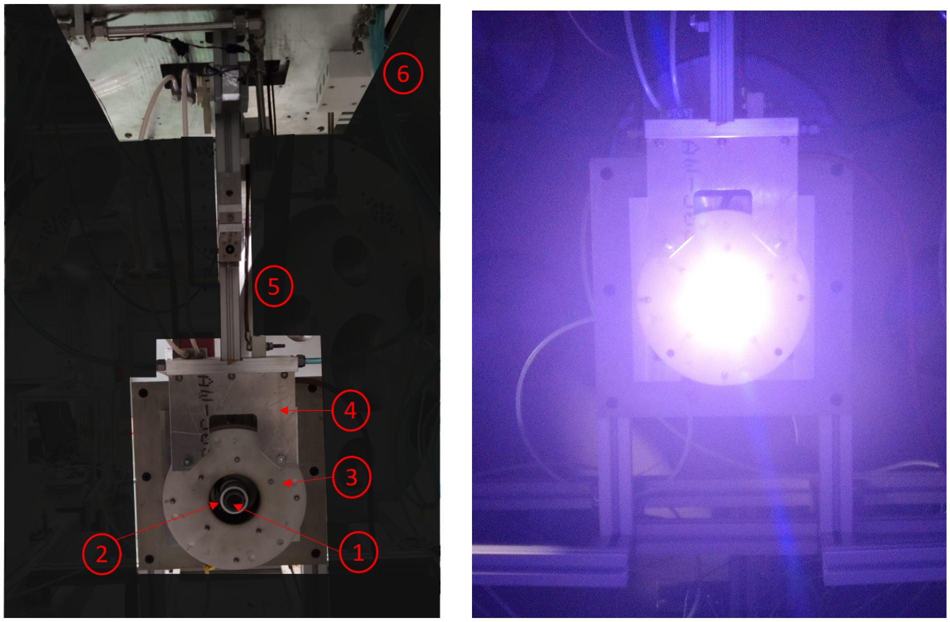

Fig. 1 Left: HIPATIA System TU-EBBM assembled on the UC3M-EP2 thrust balance. 1) Plasma discharge chamber, 2) RF antenna, 3) PM assembly, 4) structure and balance interface, 5) balance vertical arm (pendulum arm), 6) balance reference horizontal fix plane. Right: TU-EBBM assembled on the UC3M-EP2 thrust balance during a test with Krypton as propellant.

These parameters are mainly both the radiofrequency power level and the propellant mass flow rate feeding the thruster unit. This prototype, further described in Section II implements a permanent magnet assembly as the magnetic field generator, and it was designed to operate up to 600 W with a nominal working point around 450 W of incident RF power and 5-20 sccm of Xenon. In addition, the prototype, as the HPT concept it self, can work with other propellants like Argon or Krypton. For the scope of this work, some preliminary results on Krypton as an alternative to Xenon are also explored.

Although the focus of this article is to explore only the propulsive performances of the HPT - thruster unit, other units that compose the propulsion subsytem as a whole, the radiofrequency generator power unit (RFGPU) and the propellant flow control unit (PFCU) have been developed too. These have been integrated together with the thruster unit, completing the full functional chain of the propulsion subsystem. This has been enabled by the ambitious HIPATIA project (HelIcon Plasma Thruster for In-space Applications). This is of high relevance since it enables the characterization of the overall subsystem efficiency, and also at functional level how each element might impact on the actual thrust, e.g. drifts due to power tuning or transients due to the propellant flow level conditioning.

The rest of this article is organized as follows. Section II describes in detail the experimental setup, including both a brief review of the thrust balance [21], and an accurate description of the HPT thruster unit. This section also describes the methodology followed to analyze the thrust balance data: thrust balance calibration and firing sequence, i.e. how the thruster operation impacts on the recorded thrust data and which is the procedure followed to remove any disturbance such as thermal drifts. Section III presents the thrust results for the different explored operational parameters and discuss the impact at system level efficiency. Section IV wraps the important conclusions of this work.

II. Experimental setup and methodology

The HPT thruster unit (TU) elegant breadboard model (EBBM) is a prototype model based on previous breadboard designs ([11]) modified to work with a fixed magnetic field topology but it provides a certain flexibility with respect to more constrained engineering models. This TU-EBBM gives some margin on the mechanical disposition of the different constitutive elements, which will be presented next, enabling the study of different TU layouts, leading consequently to different performances depending on each configuration. The TU consists of the following main elements (see Figure

1): (1) a plasma discharge chamber or tube, made of boron nitride, 25 mm ID, where the plasma is created, confined and heated; (2) a radiofrequency inductor or antenna in charge of transferring power to the plasma and operated in the 13-14 MHz range. In this setup the antenna is a half-turn helical antenna; (3) a magnetic generator assembly, which for the EBBM is made of a PTFE structure that allocates a set of Neodymium magnets arranged within an specific configuration to generate the magnetic field topology. This magnetic field shapes a converging-diverging geometry or magnetic nozzle, being its maximum (or magnetic throat) located at the outlet of the chamber tube; (4) an aluminum structure which withstands all the elements together within the desired configuration and provides the mechanical interface to the thrust balance; neutral gas is injected from the back side of the tube, where it interfaces with the aluminum structure.

Concerning the RF power generation setup, two different systems have been tested in the frame of this work: (i) an engineering model of a custom design radiofrequency generator power unit (RFGPU) [4]; and (ii) a custom-off-the-shelve power amplifier (PA), by Seren's RF Industries, belonging to the HR 2100 series. Both amplifiers feeds the same coaxial transmission line that connects the amplifier and the TU (antenna connection), with an intermediate pi-type matching network that ensures power transfer maximization. Setup (i) is intended to validate the functional chain of the full HIPATIA system, including thre sub-systems, a DC/DC converter, the amplifier itself, and the power control hardware that would maximize power transfer, ideally, without the need of tuning the aforementioned matching network, regardless the TU operational point; the main drawback of this system is that it presents a larger uncertainty on the set/measured RF power, and since the matching network is not readjusted in the frame of this work, the measured delivered power level spreads in a wide range around the set value; the second setup (ii) which is a power amplifier for industrial RF plasmas, allows power control during the test by tuning the matching network for each specific TU load, i.e. a different impedance for each operating condition. This amplifier is also more robust in terms of its capability of managing large amounts of reflected power. Results for both power generator systems are included and discussed in Section III.

For the mass flow control, a Bronkhorst mass flow controller has been used, model EL-FLOW Select Xenon calibrated, with an accuracy of 0.1 sccm and 100 sccm full range. For the test sequences carried out with Krypton as propellant, appropriated correction factors have been applied to the set/measured mass flow rates.

All the experiments are carried out within a vacuum chamber designed specifically to characterize Electric Propulsion Plasma Thrusters up to 1.5 kW, and located at the UC3M facilities. The vacuum chamber consists of a stainless-steel 304 (non magnetized) vessel of 1.5 m inner diameter and 3.5 m long. This is equipped with three different vacuum technologies: a dry mechanical pump Leyvac LV80 with pumping speed of about 80 m^3/h, a pair of turbo-molecular pumps, Leybold MAGW2.200iP with 2000 l/s of pumping speed each, and three cryo-panels, Leyvac 140 T-V, all systems from Leybold GmbH. The total pumping speed is about 37,000 l/s Xe, reaching an ultimate pressure of 10^{-7} mbar in dry conditions. The operational pressure is roughly $2 \cdot 10^{-5}$ mbar, at 20 sccm of Xe.

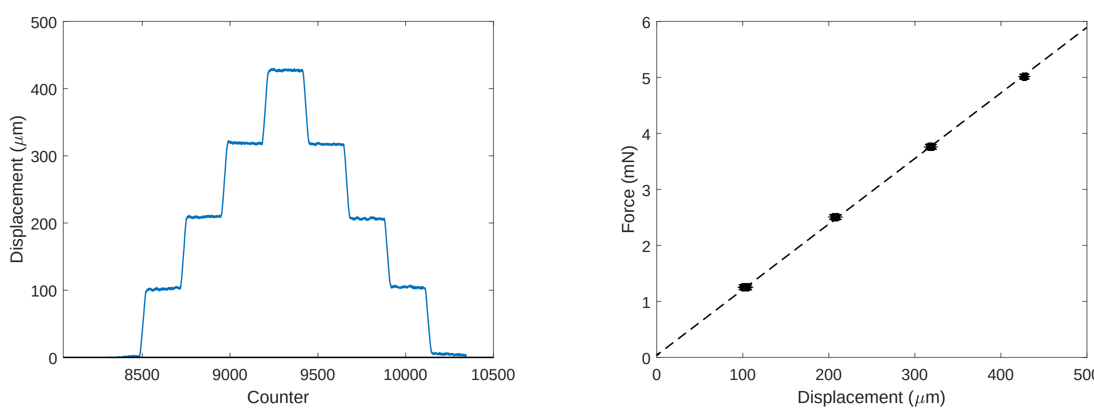

Fig. 2 Left: Calibration data (amplified displacement) retrieved from thrust balance during calibration procedure. Right: Pos-processed results, *thrust vs amplified displacement*, for the selected prototype layout.

The thrust balance used in this experiment consists of a hanging vertical pendulum with mechanical amplification based on the design of Polzin *et al* [13]. The magnified displacement is measured by means of a confocal chromatic

Table 1 Thrust test operational sequence

ID	Event	Description
1	Zero	Balance displacement measurement set to zero after previous run (if applicable), and wait for stabilization, non apparent external drifts, neither oscillations or excessive noise.
2	Ignition gas flow setup	Propellant gas flow is enabled and set to the ignition level and wait for thrust balance stabilization. This is typically a step response of some seconds
3	Thruster ignition	RF power is enabled, leading to the initial plasma discharge.
4	Flow down stage	Flow down of the propellant to the desired operational point. Due to the dynamical response of the prototype, this step could be split for different target mass flow values.
5	RF power up	After the initial propellant flow down from ignition, a power up is performed (in one or several steps) to the desired power value. This step is related to the electronic response of the plasma for different flow rates (different plasma impedance).
6	Thruster off	RF power and propellant flow are turned off. The first has a associeated an abrupt step-down, the second, it has associated a slow transient response.

sensor CCS-Prma from STIL. Then, thrust can be retrieved from this displacement once the system stiffness (i.e. k [mN/mm]) is determined through the calibration procedure. Note that the stiffness is not only determined by the balance, it is thruster setup dependent instead, it clearly depends, among other factors, on the mass of the thruster unit to be tested. Two independent calibration systems are implemented in the thrust balance. The first one is based on a voice coil which allow to apply controlled small forces, which emulates thrust, by linearly increasing the current on the coil. The second one consists of hanging calibrated weights on an auxiliary horizontal arm attached to the vertical arm; these weights produce an equivalent torque on the vertical arm, which emulates the same effect of thrust. Both calibration systems yields to the same system stiffness thus validating the consistency of thrust balance performances. Other features of the thrust balance, such as damping (to settle faster the oscillations), thermal management, power/gas feed decoupled connections, and data acquisition and control, could be found in our previous work [21].

Calibration curves are taken by default every time the TU is modified, and before and after each sequence of thrust measurements, which will be presented and analyzed in Section III. Figure 2, displays one of these calibration curves as an example to illustrate the dynamic response of the system during the calibration procedure. Based on these results it can be concluded that the thrust balance response, hanging the tested TU, is completely linear in the range of interest 0-5 mN, with an equivalent stiffness of k_{cal} = 0.0117 mN/μm (±2 %).

The thrust measurements are carried out following a predefined sequence on the TU operational parameters, i.e. order in which the power/mass flow rate are set/modified (brifly summarized in Table 1). This allows obtaining a specific dynamic response of the thrust balance, which is repeatable and reproducible for different TU firings at the same targeting operating point, thus making easier the isolation of the different operating parameters impact at thrust level and the reduction of the uncertainty associated to the thermal drift, which can be removed at post-processing time (Figure 3). This process starts with a period of balance zeroing, in which the oscillations and noise on the displacement signal are tracked to detect any anomaly (e.g. thermal drifts from previous ignitions, vibrations/displacements induced by other testing equipment's, etc.,). Once stabilized, the mass flow rate is set at the nominal point for ignition, cold gas thrust can be easily observed and measured. Then, RF power is enabled and TU ignites. Afterwards, the mass flow rate is decreased to the targeting value or to an intermediate value. Then, power is ramp up/down depending on the targeted power level. The same applies to the mass flow rate, which could present a second ramp down to the desired mass flow rate. After stabilization, the system is at its operating point, and thrust can be retrieved just by measuring the displacement and applying the proper calibration constant presented before. After a few seconds, RF is disabled and mass flow rate is set to 0. The measured displacement should reach ideally the same null reference level. However, small thermal drifts of the setup arise and these are technically unavoidable. If the time length of the test is short enough, the thermal effect only causes a small displacement drift, which can be linearized and subtracted to the measured signal, and corrected almost completely as shown in Figure 3. Note also that in this sequence the power unit that has been used is the custom made one, the RFGPU.

If the displacement is converted to thrust, according to the TB stiffness k_{cal} obtained through the calibration process, then, for the proposed sequence, the results would be the following: the cold gas effect (for the ignition mass flow rate level, 40 sccm Xe) would be about 1 mN; the power enabling event produces a peak of thrust reaching 5.3 mN (power about 225 W); this is followed by the mas flow rate ramp down to 20 sccm (3.8 mN); before reaching the steady state, the power is ramp up in three steps, producing roughly 4.4 mN of thrust at 375 W (20 sccm Xe); and then the mass flow

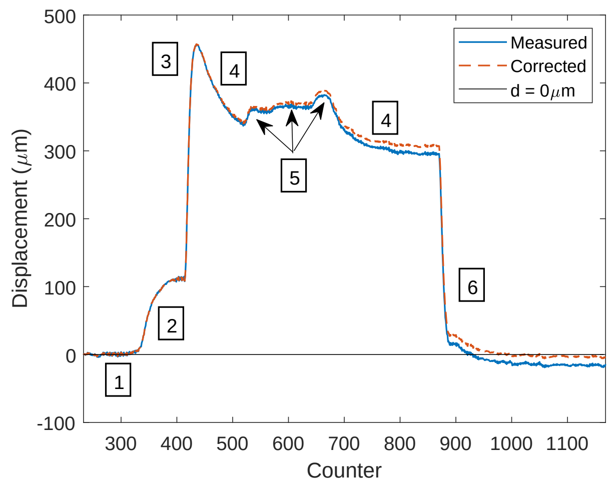

Fig. 3 Thrust test sequence. Solid line: Thrust balance output, magnified displacement (μm). Dashed line: Corrected measurement, the thermal drift is substracted to the original signal along the time period in which the trhuster is fired. The balance acquisition frequency is 10 Hz (i.e. 10 units of counter per second).

rate is decreased to the nominal point, in which thrust is 3.5 mN. Finally, RF is disabled. Since the mass flow rate is smaller at the end of the sequence, only 12.5 sccm, the measured cold gas effect is about 0.3 mN, which goes to 0 after a transient process.

III. Results Discussion

A parametric analysis of the TU propulsive performances, mainly thrust, specific impulse and thrust efficiency, is carried out for two operational parameters, (a) the propellant mass flow rate and, (b) the RF power level. The explored mass flow rate range expands from 10 sccm up to 40 sccm Xenon, being the latest the nominal mass flow rate for TU ignition. In between, multiple thrust measurements have been completed at 12.5, and 20 sccm Xenon, which would correspond theoretically to different throttling modes, low/high thrust and high/low specific impulse respectively. Although this trend is satisfied, both points remains, as it will be discussed along this section, within the undesirable low thrust efficiency range.

On the other hand, for the RF power levels, discrete values are set from 300 to 450 W, with steps of 50 W, whenever the PA is used. For the RFGPU scenario, the estimated RF power introduced to the system ranges from 200 to 430 W, with a non-uniform spacing because of the functional constraints inherent to the electronics architecture, as briefly described in Section II.

Figures 4 summarize the TU performances when it is coupled to the RFGPU electronics (i). The first graph plots the thrust versus the incident power level, at three different mass flow rates (40, 20 and 12.5 sccm). For each operating point, the thrust level is obtained by averaging each step over time after subtracting the small effect of the *linear* thermal drift as explained in the previous section. For this setup (i) most of the results are gathered after concluding the ramp down to 20 sccm of Xe, where a linear trend of the thrust response with power could be identified. This allows concluding that thrust increases with power at 20 sccm of Xe. For the ignition mass flow rate, i.e. 40 sccm, a wider dispersion in the thrust measurement was observed. During ignition, power had never been set to higher levels due to the constrains imposed by the control protocol of the electronics, so no trend has been identified. But this uncertainty will be reduced an complemented later with the additional data reported using the second setup (ii). For the lower mass flow rate, 12.5 sccm, thrust with setup (i) is only available at higher incident powers, and no trend can be found. Besides, at that Xenon level a high repeatability of the measurements was observed for the nominal value around 430 W. Wrapping up the thrust results for setup (i), the higher the mass flow, the higher the obtained thrust. A conclusion that agrees with the expected response where the increase of neutral gas imply an overall increase of ions (i.e. higher ion beam current), despite the loss in acceleration, as already reported in previous testing campaigns ([5], [14]. The thrust efficiency, traditionally

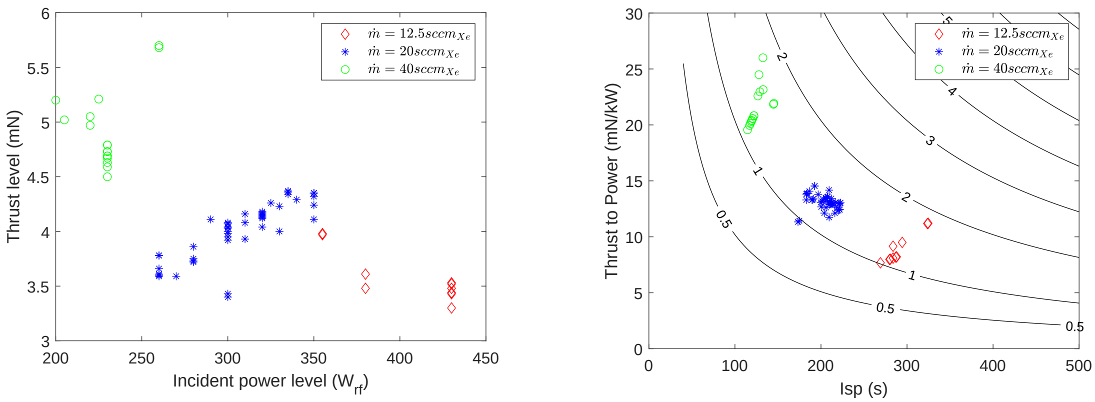

Fig. 4 Thrust performance results for setup (i) with RFGPU. Left: Thrust level at different incident power values. Right: Thrust to power level and specific impulse results. Contour lines indicate the thrust efficiency (in %).

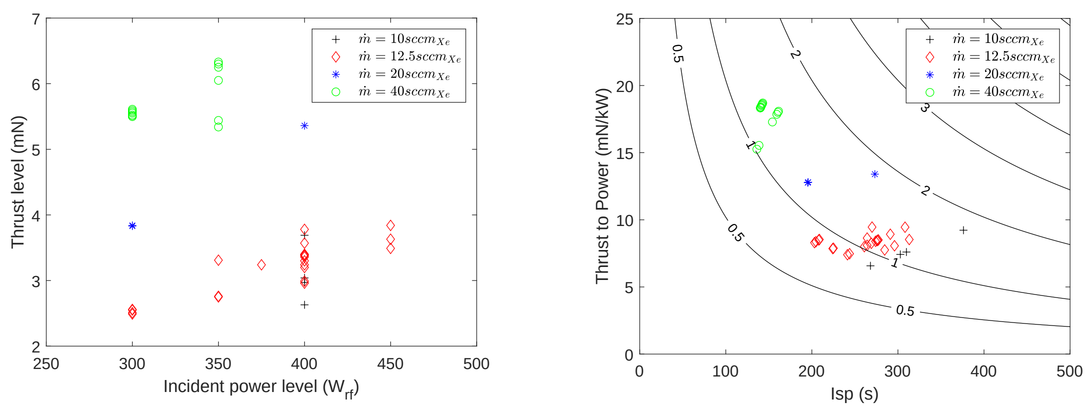

Fig. 5 Thrust performance results for setup (ii) with PA. Left: Thrust level at different incident power values. Right: Thrust to power level and specific impulse results. Contour lines indicate the thrust efficiency (in %).

defined as $\eta = F^2/2\dot{m}P$, remains quite low for all the operating conditions, as illustrated in the right hand side graph of Figure 4. F, $\dot{m}$ and P, stand for thrust, mass flow rate and power into the system respectively. The results are plotted in a graph of thrust-to-power ratio F/P versus the specific impulse $I_{sp} = F/\dot{m}$. In this plot, constant-efficiency contours are overlapped with the scattered data, and the lines of 1 and 2 % efficiency bounds all the results. Ion velocity increases with the reduction of mass flow rate, but penalizing on F/P, This increase in ion energy, for the HPT technology, correlates well with an increase of both, the propellant utilization ($\eta_u = I_{i,beam}$ / $e\dot{m}$, with $I_{i,beam}$ the total ion beam current and e the electron charge) and the electron temperature, which agrees well with the ambipolar field limited drop predicted by Martínez-Sánchez *et al* [9]. Note that I_{sp} ranges from 100 to 350 sec approximately, which is a very poor result, comparable to that of classical chemical rockets. This can be explained by the fact that for all the explored range, this prototype lacks of reaching high utilization efficiencies above 50 %, and the temperature, although not presented in this work, has been estimated to be lower than 3-4 eV.

For the setup (ii), analogous results are depicted in Figure 5. This setup behaves more stably in comparison to (i), specifically at lower mass low rates, being possible to decrease it down to 10 sccm. This allows exploring easily the trend of thrust with incident power at 12.5 sccm of Xenon, resulting again a linear trend. A few thrust measurements were taken at 20, 40 sccm to compare the performances of this power setup against (i). Regarding the thrust efficiency,

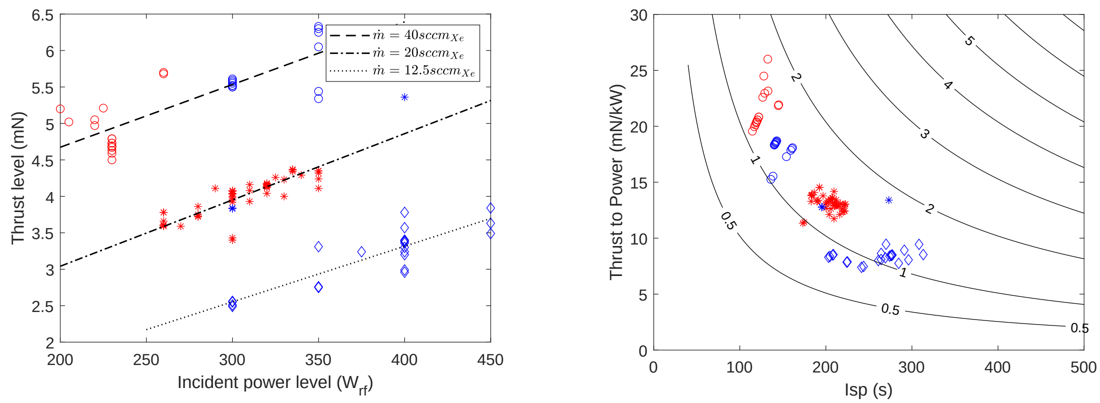

Fig. 6 Thrust performance results comparing previous results in Figures 4 and 5.The best linear fit $T - P$ is presented at each $\dot{m}$ level (data belonging to RFGPU at $\dot{m} = 12.5sccm_{Xe}$ has been excluded). Right: Thrust-to-power vs specific impulse for all the explored parametric range, with both electronics: in red (RFGPU) in blue (PA).

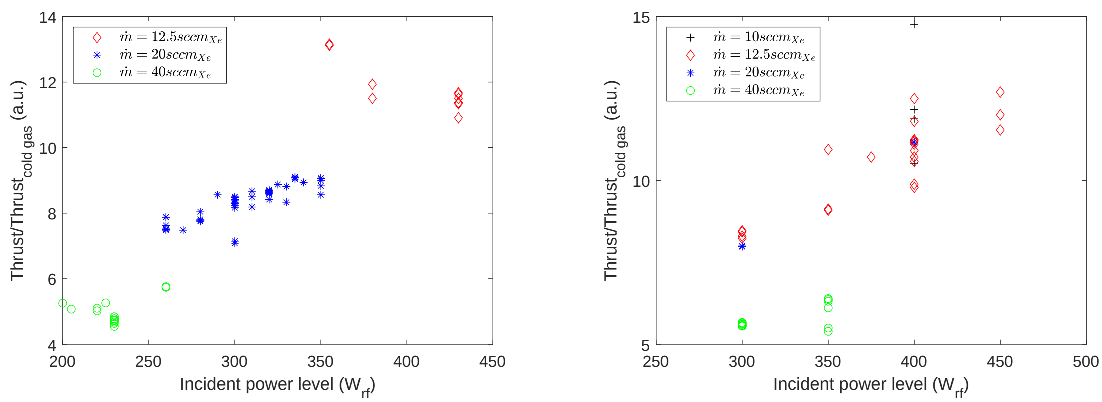

Fig. 7 Dimensionless thrust gain with respect to reference cold gas value. Left: RFGPU, right: PA.

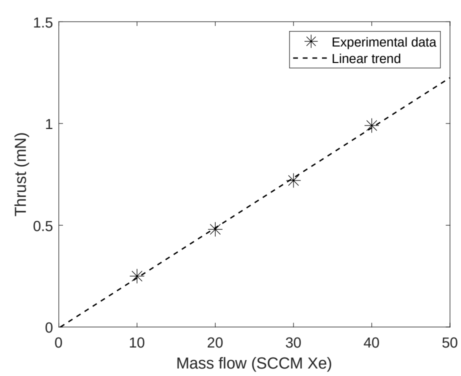

Fig. 8 Cold Gas thrust response characterization.

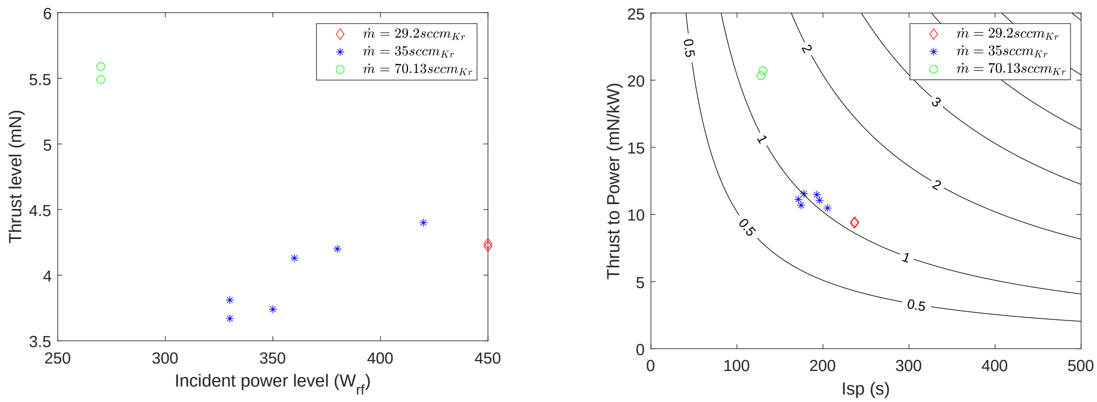

Fig. 9 Thrust performance results for Krypton. Left: Thrust level at different incident power values. Right: Thrust to power ratio vs specific impulse results. Contour lines indicate the thrust efficiency (in %).

this is bounded withing the 1-2% range, concluding that the TU behaves similarly with both electronics. This means that the results presented here validate the customized RFGPU at TRL4-5 and it supposes a step forward towards the consolidation of the HIPATIA system. The coherent result of both setups can be checked in Figure 6, in which the same linear fit of F vs P is valid for the different mass flow rates along the evaluated power range for both (i) and (ii) measurements.

Although the efficiency of the tested prototype is low, it is worthy to evaluate which is the relative increase in thrust that corresponds to the plasma with respect to that of the cold gas effect, F/F_c. This is depicted in Figure 7 for both setups. And the result is coherent with the previous reasoning, the lower the mass flow rate, the higher the utilization, the higher the temperature, and the higher the gain of thrust with respect to the cold gas. This gain in thrust increases linearly with power, e.g. for 20 sccm with setup (i) and 12.5 sccm for setup (ii). For 12.5 sccm and 400-450 W of power, the thrust gain would be about 12 or 13 times the cold gas thrust. For the lowest mass flow rate, 10 sccm, and 400 W, tested with setup (ii), the results presents a large dispersion, but the gain gactor is close to 15. On the other side, at 20 sccm, the gain factor drops below 10, and at 40 sccm, below 6. This gain factor increases with power and flow reduction, because a higher fraction of the gas is ionized, and the power is more effectively coupled on that larger fraction of ionized gas, i.e. the energy per accelerated particle is larger. Nevertheless, note that in absolute terms the thrust increases with mass flow rate, as well as the cold gas effect, as shown in Figure 8.

To complete this analysis, Figure 9 depicts the thrust results when the TU is fed with Krypton as the propellant and only using RFGPU electronics. For such a gas, the mass flow rates are about 70 sccm (for ignition), 35 sccm (intermediate mass flow rate), and 29 sccm (lowest mass flow rate). Most of the results belong to the intermediate mass flow rate, for which the linear trend with power is recovered. The thrust efficiency for the Krypton tests seems to be slightly lower, close to 1.1-1.2 % in average.

Wrapping up all the previous results we are in front of an HPT prototype which provides poor propulsive performances. This suppose a step backward with respect to previous prototypes that shown higher performances with indirect thrust estimation, [10], [11]. Nevertheless, former prototypes were operated below 10 sccm, a level which cannot be reached consistently with the current TU prototype. Consequently, a fair comparison cannot be carried out. With some support of plasma probes measurements (Faraday cup, compensated Langmuir probe, and a retarding potential analyzers), the low efficiency can be linked without no doubt to the low propellant utilization and the inefficiency on producing a high energetic ion beam. The additional power is converted only partially into thrust, and part of it is converted into thermal loads to the plasma discharge chamber. The last issue can be explained by the inappropriate magnetic field topology design of the permanent magnet assembly. This magnetic field also shows some difficulties to couple properly the power from the RF inductor, an effect which is noted as the incapability of reducing the mass flow rate below 10-12.5 sccm, regardless the power injected is as high as 450 W.

IV. Conclusions

The first set of consolidated thrust measurements for the HIPATIA System TU have been presented. The results show a very low thrust efficiency, below 2%, with moderate thrust level, up to 6.5mN and a low specific impulse, less than 400 s. The work has been useful to validated the functional performances of the RFGPU power unit against a commercial power amplifier. The increase of thrust with mass flow rate and power has been identified, as well as the increase of specific impulse with the reduction of propellant flow. This increase does not impact positively in the thrust efficiency, consequently, energy losses due to ionization/excitation and plasma-wall interaction increases as well counteracting the aforementioned thrust gain. It has been pointed out that the current prototype magnetic field yields to a weaker plasma-wave power coupling, in comparison to former prototypes, which were tested at much lower mass flow rates with great success, with higher utilization efficiencies, higher electron temperatures and higher ion beam energies. For this reason, as future work, a detailed comparison between the different HPT models will be carried out to identify the advantages/drawbacks of each one in order to establish the road map for the design of new thruster units.

Acknowledgments

This project has received funding from the European Union's Horizon 2020 research and innovation program under grant agreement No 870542 (HelIcon PlasmA Thruster for In-space Applications). The authors acknowledge the effort of all those people involved in the development of the RFGPU electronics at Sener Aeroespacial, specially, Amadeo Velasco and Álvaro Gimenez, and in the iteration of the mechanical implementation of the TU, Cándido Garrido.

References

[1] S. Cheng and M. Martinez-Sanchez. "Modeling Of Hall Thruster Lifetime And Erosion Mechanisms". In: *30th International Electric Propulsion Conference, Florence, Italy*. IEPC-2007-250. 2007.

[2] O.B. Duchemin. "An investigation of ion engine erosion by low energy sputtering". PhD thesis. California Institute of Technology, Pasadena, CA, 2001.

[3] C.E. Garner, J.R. Brophy, and J.E. Polk. "Cyclic Endurance Test of a SPT-100 Stationary Plasma Thruster". In: *30th Joint Propulsion Conference, Indianapolis, IN*. AIAA 1994-2856. 1994.

[4] V. Gómez et al. "RF power-plasma coupling experimental results in a helicon plasma thruster prototype". In: 36^{th} *International Electric Propulsion Conference*. IEPC-2019-365. Vienna, Austria: Electric Rocket Propulsion Society, 2019.

[5] Pablo Fajardo; Mario Merino; Eduardo Ahedo; Vıctor Gómez; Mercedes Ruiz Jaume Navarro-Cavallé; Mick Wijnen. "Experimental performances of a 1kW HPT by means of plasma diagnosis". In: *35th International Electric Propulsion Conference*. IEPC-2017-447. Atlanta, Georgia, USA, 2017. URL: `http://ep2.uc3m.es/assets/docs/pubs/conference_proceedings/nava17.pdf`.

[6] I. Katz et al. "Ion Thruster Life Models". In: *41st AIAA/ASME/SAE/ASEE Joint Propulsion Conference and Exhibit*. AIAA 2005-4256. 2005.

[7] JM Little and EY Choueiri. "Critical condition for plasma confinement in the source of a magnetic nozzle flow". In: *IEEE Transactions on Plasma Science* 43.1 (2014), pp. 277–286.

[8] M. Martínez-Sánchez and J.E. Pollard. "Spacecraft Electric Propulsion — An Overview". In: *Journal of Propulsion and Power* 14.5 (Sept. 1998), pp. 688–699. ISSN: 0748-4658. DOI: 10.2514/2.5331.

[9] Manuel Martínez-Sánchez, Jaume Navarro-Cavallé, and Eduardo Ahedo. "Electron cooling and finite potential drop in a magnetized plasma expansion". In: *Physics of Plasmas* 22.5 (2015), p. 053501.

[10] J Navarro-Cavallé et al. "Experimental characterization of a 1 kW helicon plasma thruster". In: *Vacuum* 149 (2018), pp. 69–73.

[11] Jaume Navarro-Cavallé et al. "Development and Characterization of the Helicon Plasma Thruster Prototype HPT05M". In: 36^{th} *International Electric Propulsion Conference*. IEPC-2019-596. Vienna, Austria: Electric Rocket Propulsion Society, 2019.

[12] D. Packan et al. "The MINOTOR H2020 project for ECR thruster development". In: 35^{th} *International Electric Propulsion Conference*. IEPC-2017-547. Electric Rocket Propulsion Society, 2017.

[13] Kurt A Polzin et al. "Thrust stand for electric propulsion performance evaluation". In: *Review of Scientific Instruments* 77.10 (2006), p. 105108.

[14] Jaume Navarro-Cavallé; Mick Wijnen; Pablo Fajardo; Eduardo Ahedo; Vctor Gómez; Álvaro Giménez; Mercedes Ruiz. "Test campaign results of a Helicon Plasma Thrauster (HPT-05M) prototype and its future development plan." In: *Space Propulsion Conference 2018*. SP2018-290. Seville, Spain, 2018.

[15] M. Umair Siddiqui et al. "First Performance Measurements of the Phase Four RF Thruster". In: *35th International Electric Propulsion Conference, Atlanta, GA*. IEPC-2017-431. 2017.

[16] K. Takahashi, Y. Igarashi, and T. Fujiwara. "Plane and hemispherical potential structures in magnetically expanding plasmas". In: *Applied Physics Letters* 97 (2010), p. 041501.

[17] K. Takahashi et al. "Electron Diamagnetic Effect on Axial Force in an Expanding Plasma: Experiments and Theory". In: *Physical Review Letters* 107.23 (2011), p. 235001.

[18] Kazunori Takahashi. "Magnetic nozzle radiofrequency plasma thruster approaching twenty percent thruster efficiency". In: *Scientific reports* 11.1 (2021), pp. 1–12.

[19] Kazunori Takahashi et al. "Commentary: On helicon thrusters: Will they ever fly?" In: *Frontiers in Physics* 8 (2020), p. 277. ISSN: 2296-424X. DOI: 10.3389/fphy.2020.00277.

[20] E. Toson et al. "Development and Testing of a Miniature Helicon Plasma Thruster". In: *35th International Electric Propulsion Conference, Atlanta, GA, IEPC-2017-519*. 2017.

[21] M. Wijnen, J. Navarro-Cavallé, and P. Fajardo. "Mechanically amplified milli-newton thrust balance for direct thrust measurements of electric thrusters for space propulsion". In: *IEEE Transactions on Instrumentation and Measurement* 70 (2021), p. 3505318.